Angled fiber-based Fabry-Perot interferometer

XINPU ZHANG,[1,*] LIXIA LI,[2] XIHUA ZOU,[1] BIN LUO,[1] WEI PAN,[1] LIANSHAN YAN,[1] QIANG WU[3]

[1] *Center for Information Photonics and Communications, School of Information Science and Technology, Southwest Jiaotong University, Chengdu, Sichuan 611756, China*
[2] *School of Physics, Henan Normal University, Xinxiang, Henan 453007, China*
[3] *Faculty of Engineering and Environment, Northumbria University, Newcastle Upon Tyne, NE1 8ST, United Kingdom*
**Corresponding author: xpzhang@home.swjtu.edu.cn*

Received XX Month XXXX; revised XX Month, XXXX; accepted XX Month XXXX; posted XX Month XXXX (Doc. ID XXXXX); published XX Month XXXX

Herein, we proposed and experimentally demonstrated a novel all-fiber Fabry-Perot (FP) interferometer which is formed by a simple angled fiber which can function as a beam splitter. According to the principle of the angled fiber, we verify the influence of oblique angle on light propagation path and light intensity ratio. Subsequently, angled fiber-based FP interferometers are experimentally demonstrated, and the influence of oblique angle on the visibility of interference fringes and temperature characteristics is investigated. Finally, the temperature characteristics of this proposed FP interferometer is investigated experimentally, the temperature sensitivity is 12.62 and 10.89pm/°C for 42 ° and 40 ° angled fiber-based fiber FP interferometer, respectively. This proposed FP interferometer is fabricated by using a simple angled fiber, which has advantages of ease fabrication and all-fiber characteristic, and hence can meet the requirements of mass production and high stability in various practical application areas.

OCIS codes: *(060.2370) Fiber optics sensors; (060.2340) Fiber optics components; (050.2230) Fabry-Perot; (280.6780) Temperature.*

http://dx.doi.org/10.1364/OL.99.099999

In a sense, the miniaturization of optical systems and devices is the development trend, meanwhile, it is of great significance to seek an effective and efficient way to develop integrated optics and integrated photonic devices or chips. Currently, miniaturization of photonic devices is being intensively focused because they drive great scientific and technological developments in the fields of optical communications, bio-photonics, photonic integrations, and microwave photonics [1, 2]. Among different photonic components, fiber optic components can provide excellent platforms for integrated optic system and integrated photonic devices. Although, most fiber optic components have simple functions and are used as discrete devices in optics system, which still play an important role in promoting integrated optics.

Significantly, because of their versatile characteristics and excellent one-dimensional structural properties, fiber components have attracted considerable attention as building blocks for important elements of integrated photonic devices, including photodetector [3], optical switching [4], fiber laser [5], single photon source [6], micro-prism [7], and fiber sensor [8]. So far, with the development of integrated photonic systems, due to the inherent characteristics of compact structure and stability of the fiber optic components, fiber passive devices are usually used to the seamlessly integrated coupling construction between miniaturized photonic devices and conventional fiber optical system [9]. Most commonly, the coupling between fiber optical system and photonic chip can be realized by using the optical fiber micro-lens or angled fiber [10], besides fiber micro-lens or angled fiber-assisted coupling, fiber micro-lens and angled fiber also have great application prospects in the field of space optics [11] and fiber sensing [12].

As fiber sensors, high sensitivity, immunity to electromagnetic interference, low cost and compact size, are some of their most attractive features. In optical fiber sensing, fiber Fabry-Perot (FP) interferometers, especially fiber tip FP interferometers, have been attractive for a wide range of applications because they have many distinctive advantages over traditional FP interferometers, such as more miniature size. Recently, the angled fiber-based miniature fiber FP interferometer has been proposed [12], however, the purpose of introducing an angled fiber, according to design principle, is only to steer the optical axis based on internal reflection at the angled fiber end face instead of playing the role of beam splitter, and the more important functions of the angled fiber is almost completely neglected in this scheme.

In this paper, in order to get all the advantages of the angled fiber components, a novel all-fiber FP interferometer is experimentally demonstrated. This proposed fiber FP interferometer is formed by a simple angled fiber. The angled fiber is made by end-face polishing process, which is an effective method to control the oblique angle. Due to the splitting characteristic of the angled fiber, the different oblique angles are corresponding to different light propagation path and light intensity ratio. Thus, while an angled fiber constitutes a FP interferometer, the light intensity ratio between the interference beams, can be adjusted flexibly by controlling the

oblique angle of the angled fiber. Finally, the angled fiber-based FP interferometer with different visibility of fringe can be realized by this simple, reproducible and stable scheme. Experimentally, this proposed FP interferometer is fabricated, and the influence of oblique angle on the visibility of interference fringes and temperature characteristics is investigated, and the temperature response is verified by measuring the spectrum shift.

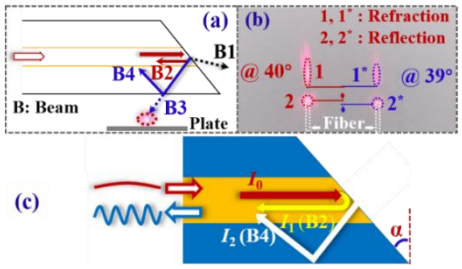

Fig. 1. (a) Schematic illustration of splitting characteristic of angled fiber, (b) Reflection vs different oblique angles, a 40 ° and 39 ° angled fiber is investigated by a red light. The output light reflected by the angled fiber end is observed in the sidewise direction, and the reflection direction from different angles demonstrate that different angles correspond to different reflection paths and reflection intensity, (c) Illustration of angled fiber-based FP interferometer.

The beam splitting operating mechanism of the angled fiber is schematically shown in Fig. 1(a). As shown, for an end polished fiber, the oblique angle directly determines the propagation path and the form of light. When the oblique angle is greater than or equal to the critical angle, the optical axis can be steered based on total internal reflection at fiber end face [13], and most of the light will escape out of the cladding. Nevertheless, for the oblique angle small than the critical angle, when incident light arrives at the fiber-air interface, the light splits into four portions: Firstly, the most incident light is refracted by the fiber end-face, and escape from the fiber (B1); Secondly, slight incident light changes from forward-propagating light to return light (B2) caused by the overlap of reflected light and guide mode field, thus, it mainly depends on fiber end angle and end diameter, and it is the root cause of return loss. The return light stems from the Fresnel reflection at the fiber-air interface, although the reflection direction seriously deviates from the axis of the fiber, it also can cause poor coupling into the guided mode of the fiber, and the coupling efficiency of the reflected beam into the guided mode is mainly depended on the oblique angle [14]; Thirdly, besides the return light, due to the angled end-face, the optical axis is steered, the residual light reflected by the oblique fiber-air interface, will enter into the cladding and most of the reflected light will escape from the fiber cladding (B3), meanwhile, some of the reflected light will be reflected by cladding-air interface and recouple into the guided mode of the fiber (B4) , which caused by the overlap integration of reflected light and guided mode.

Subsequently, in order to verify the mentioned splitting operating mechanism of the angled fiber, we fabricate two angled (40 ° and 39 °) fibers with different oblique angles. The two angled fibers investigated by a red light is shown in Fig. 1(b). Figure 1(b) is overhead view, the refraction and reflection light are corresponding to B1 and B3 in Fig. 1(a), respectively. Significantly, the intensity ratio between the refraction and reflection light and propagation path from the angled fiber with 40° oblique angle is obviously different from that from the angled fiber with 39° oblique angle. That is, the different propagation path and splitting ratio represents the different angled fiber [13].

Figure 1(c) shows the operating mechanism of this proposed angled fiber-based FP interferometer. As shown, the return light I_1 (Corresponding to B2) originates from the weak coupling between the reflected light (which is reflected by the Fresnel reflection at the fiber-air interface) and guided mode. The rest of the reflected light is injected into the cladding, when it arrives at the cladding-air interface, it is partly reflected and recoupled into the fiber core (I_2, corresponding to B4). Then, light I_1 (B2) interferes with light I_2 (B4), and the interference fringes can be observed in the reflection.

Traditionally, for this proposed FP interferometer, in order to facilitate the analysis and design, the interference can be modeled as a two-light interference process, for which the interferometric light intensity can be expressed as:

$$I = I_1 + I_2 + 2\sqrt{I_1 I_2}\cos\left(\frac{4\pi\left(n_2 l_2 - n_1 l_1\right)}{\lambda} + \phi_0\right) \quad (1)$$

where n_1 and n_2 is the effective refractive index of fiber materials which B2 and B4 passed by, respectively. l_1 and l_2 is the propagation length of B2 and B4, respectively, and ϕ_0 is initial phase difference.

While two beams meet the coherence conditions, the visibility of fringe V is given by:

$$V = \frac{I_{Max} - I_{Min}}{I_{Max} + I_{Min}} = \frac{2\sqrt{I_1 I_2}}{I_1 + I_2} \quad (2)$$

Assuming $R = I_2/I_1$, thus,

$$V = \frac{2\sqrt{R}}{1+R} \quad (3)$$

According to Eq. (3), for a two-light FP interferometer, the visibility of fringe is dependent on the ratio of the intensity of two light. Obviously, the visibility of fringe increases with the decreasing intensity difference between two light.

In accordance with the above analysis, the angled fibers with different oblique angles are corresponding to different propagation path and light intensity ratio. For this angled fiber-based FP interferometer, the light intensity and propagation path of B2 and B4, which are interference beams, can be adjusted by controlling the oblique angle of the angled fiber. Finally, the angled fiber-based FP interferometer with different visibility of fringe can be realized by this simple, reproducible and stable scheme.

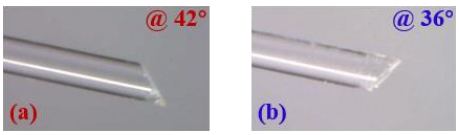

Fig. 2. Microscope photographs of angled fibers with different angles. (a) 42°-angled fiber, (b) 36°-angled fiber.

In order to demonstrate the feasibility of this angled fiber-based FP interferometer, the angled fiber with different oblique angles is fabricated by using a bare fiber polisher (*Krell Technologies Inc.*, *Radian*), which can provide the ability to polish optical fibers at selectable and variable angles. This bare fiber polisher has an angle range of 0 ° to 45 °, angle tolerance of typically ±0.5 °, which can provide the high-flatness end-face and high-precision polishing. According to the aforementioned principle, the angled fiber-based FP interferometer with different visibility of fringe can be realized

by simple fiber polishing, therefore, the angled fibers with different oblique angle are prepared. Figure 2(a) and 2(b) show the microscope photographs of two angled fibers with 42 ° and 36 ° oblique angle, respectively. It can be seen that the precise controlling of the fibers' oblique angle can be realized based on high-precision polishing, and the end-face of the angled fibers is approximately smooth. The reason that the oblique angle is in need of precise control as the oblique angle has a significant influence on the property of the angled fiber.

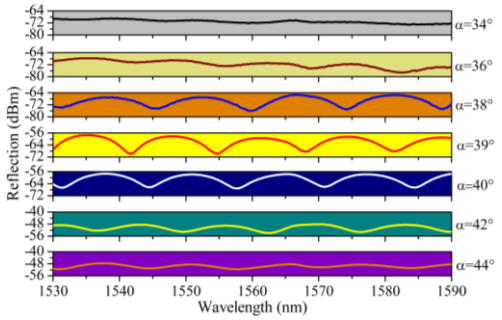

Fig. 3. Spectrum evolution of fiber FP interferometer versus angles.

After the above analysis, the theoretical splitting characteristic of the angled fiber is demonstrated, and the simulation results are shown in Fig. 4(a). From Fig. 4(a), it can be observed that the angled fibers with different oblique angles are corresponding to different propagation path and splitting ratio. Thus, the angled fiber can be used to constitute fiber FP interferometer with variable visibility of fringe, and the performance of fiber FP interferometer is depended on the characteristics of the angled fiber. Experimentally, to verify the operating mechanism and characteristics of this proposed FP interferometer, we fabricate the FP interferometers with different oblique angles, and investigate their spectral characters. Figure 3 shows the reflection spectra of FP interferometers with 34 °, 36 °, 38 °, 39 °, 40 °, 42 °, and 44 ° oblique angles, respectively. As shown in Fig. 3, the angled fiber-based FP interferometer with different oblique angle shows different visibility of interference fringe. Obviously, the visibility of interference fringe increases with the increasing the oblique angle while the oblique angle increases from 34° to 39°, however, as oblique angle increases from 39° to 44°, the visibility of interference fringe gradually decreases. From the experimental results, it can be deduced that the different visibility of interference fringe is caused by the angled fiber with different oblique angles corresponding to different light intensity ratios, eventually, the two beams with different intensity interferes with each other, which is consistent with Eq. (3).

To verify the impacts of R ($R=I_2/I_1$) on the visibility of interference fringe, the simulation should be implemented. Figure 4(b) and 4(c) shows the simulated relationship between visibility and R ($R=I_2/I_1$) and the experimental relationship between fringe visibility and angles, respectively. Herein, the light intensity depends on the oblique angle, the oblique angles directly determine the light intensity ratios and R ($R=I_2/I_1$). As shown in Eq. (3), for a two-light interference process, while the light intensity is closer to each other, the maximum visibility of interference fringe can be obtained, Figure 4(b) and 4(c) depict and demonstrate this phenomenon, and Figure 4(b) and 4(c) show that theoretical calculation and experimental results agree well with each other, and the visibility of interference fringe changes with oblique angle.

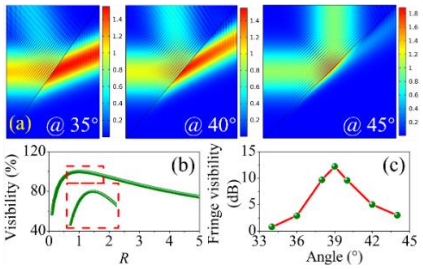

Fig. 4. (a) Theoretical splitting characteristic of the angled fiber, (b) Simulated relationship between visibility and R. Inset: Magnified region of the curve between visibility and R outlined in (b), (c) Experimental relationship between fringe visibility and oblique angles.

Subsequently, the temperature response of this angled fiber-based FP interferometer will be investigated, before experiment, the theoretical analysis should be implemented to verify the temperature characteristics. Figure 5 shows the schematics of temperature response of fiber FP interferometer.

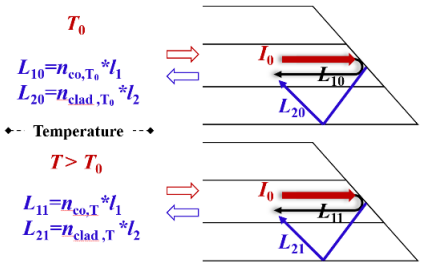

Fig. 5. Schematics of temperature response of fiber FP interferometer.

While the original temperature sets as T_0, in Eq. (1), assuming $\phi_0=0$, for a certain spectrum dip, the phase difference is given by:

$$\frac{4\pi\left(L_{20}-L_{10}\right)}{\lambda}=\frac{4\pi\left(n_{clad,T_0}l_2-n_{co,T_0}l_1\right)}{\lambda}=\left(2m+1\right)\pi \quad (4)$$

where L_{10} and L_{20} is the initial optical path of the B2 and B4, respectively. l_1 and l_2 is the initial propagation length of the B2 and B4, respectively. $n_{clad,T0}$ and $n_{co,T0}$ is the initial refractive index of fiber cladding and core, respectively. m is an integer. Thus, the wavelength of the dip λ_m is:

$$\lambda_m=\frac{2\left(n_{clad,T_0}l_2-n_{co,T_0}l_1\right)}{m} \quad (5)$$

When the FP interferometer is subjected to external temperature perturbations (T, $T>T_0$), the wavelength shift is:

$$\Delta\lambda_m=\frac{2\left(n_{clad,T}l_2-n_{co,T}l_1\right)}{m}-\frac{2\left(n_{clad,T_0}l_2-n_{co,T_0}l_1\right)}{m}$$
$$=\frac{2l_2\left(n_{clad,T}-n_{clad,T_0}\right)-2l_1\left(n_{co,T}-n_{co,T_0}\right)}{m} \quad (6)$$

where $n_{clad,T}$ and $n_{co,T}$ is the refractive index of fiber cladding and core after temperature change (From T_0 to T), respectively.

Since the thermo-optic coefficient of the fiber is one order higher than the thermal expansion coefficient, and the thermo-optic coefficient of fiber core (Germanosilicate-core, 1.15×10^{-5}/°C) is slightly higher than that of fiber cladding (Silica, 1.0×10^{-5}/°C) [15],

while temperature increases, the refractive index of fiber core is changing more than that of the refractive index of fiber cladding, but the difference between the refractive index of fiber cladding and core will be enlarged with the propagation length difference Δl between l_1 and l_2. Ultimately, as the increasing temperature, the spectrum of this angled fiber-based FP interferometer will have significant redshifts, and the angle will affect the sensitivity $\boldsymbol{S}$ of this proposed FP interferometer, which can be expressed as follow:

$$\begin{aligned} &\because\ T\uparrow\ \ \therefore\ n_{clad}\uparrow,\ n_{co}\uparrow, \\ &\because\ For\ \ \alpha\subseteq\left(30^{\circ},45^{\circ}\right),\ \left[\Delta l=l_2-l_1\right]\subseteq\left(l_2,2l_2\right), \\ &\therefore\ l_2\left(n_{clad,T}-n_{clad,T_0}\right)-l_1\left(n_{co,T}-n_{co,T_0}\right)>0,\ and\ \Delta\lambda_m>0, \\ &Also,\ \alpha_1>\alpha_2\rightarrow\left[\Delta l_1=\left(l_2-l_1\right)_1\right]>\left[\Delta l_2=\left(l_2-l_1\right)_2\right]\rightarrow S_1>S_2 \end{aligned} \tag{7}$$

To verify the temperature response of this angled fiber-based fiber FP interferometer, we experimentally calibrated and tested the temperature responses of the proposed FP interferometer with 40 ° and 42 ° oblique angle by using a lab-scale temperature measurement system. The FP interferometer probe is put into a programmable temperature-controlled box for temperature testing, and a thermocouple is used for temperature calibration near the FP interferometer; both of them are placed in the middle of the chamber. We characterized the temperature performance by tracking the dips of reflection spectra from the FP interferometer. The temperature was increased from 100 °C to 500 °C with a temperature interval of 50 °C.

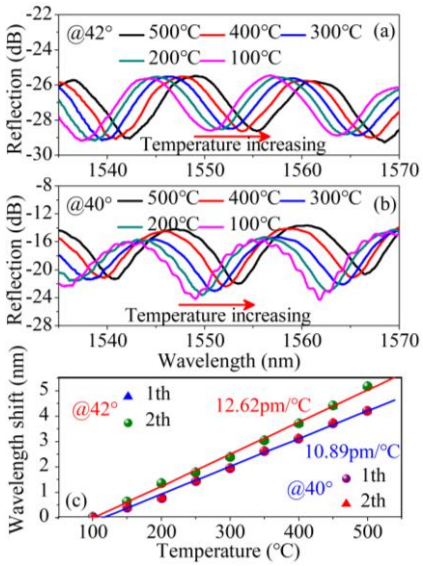

Fig. 6. Red shift of the fringes at different temperatures for the fiber FP interferometer with oblique angles of (a) 42 ° and (b) 40 °, (c) Wavelength shift as a function of temperature.

Figure 6 (a) and (b) presents the reflection spectra of the FP interferometer versus temperature variations at 100 °C, 200 °C, 300 °C, 400 °C, and 500 °C. As temperature increases, the reflection spectra of the FP interferometers shift toward long wavelength. In addition, Fig. 6(a) and (b) illustrates that the reflection spectra shifted linearly as the increasing temperature, which is coincident with Eq. (7). As shown in Fig. 6 (c), when the temperature changes between 100 °C and 500 °C, from the linear fit, the temperature sensitivity is 12.62 and 10.89 pm/°C for 42 ° and 40 ° angled fiber-based fiber FP interferometer, respectively. Experimental results show that the FP interferometers with different angles have different temperature sensitivity, which is consistent with Eq. (7).

In summary, we proposed and experimentally demonstrated a novel fiber tip FP interferometer which is formed by a simple angled fiber end. According to beam splitting of the angled fiber, we verify the influence of oblique angle on light propagation path and light intensity ratios. Subsequently, this angled fiber-based FP interferometer is experimentally demonstrated, and the influence of oblique angle on the visibility of interference fringe and temperature characteristics is investigated. Finally, the temperature characteristics of this proposed FP interferometer is investigated experimentally, and the temperature sensitivity is 12.62 and 10.89 pm/°C for 42 ° and 40 ° angled fiber-based fiber FP interferometer, respectively. Future work will be focused on sensor optimization and packaging to further enhance and optimize sensor performance.

Funding. National Natural Science Foundation of China (61705189, 61735015), Fundamental Research Funds for the Central Universities (2682017CX095) and 111 Plan (B18045).

Acknowledgement. We would like to acknowledge Wei Peng and Qiang Liu (Dalian University of Technology) for technical assistance on the high temperature measurement.

Disclosures. The authors declare no conflicts of interest.

References

1. R. X. Yan, J. H. Park, Y. Choi, C. J. Heo, S. M. Yang, L. P. Lee, and P. D. Yang, Nat. Nanotechnol., **7**, 191 (2012).
2. R. X. Yan, D. Gargas, and P. D. Yang, Nat. Photon., **3**, 569 (2009).
3. J. H. Chen, Q. Jing, F. Xu, Z. D. Lu, and Y. Q. Lu, Optica, **4**, 835-838 (2017).
4. P. C. Debnath, S. Uddin, and Y. W. Song, ACS Photon., **5**, 445 (2018).
5. F. M. Xie, N. Yao, W. Fang, H. F. Wang, F. X. Gu, and S. L. Zhuang, Photon. Res., **5**, B29 (2017).
6. T. Schröder, A. W. Schell, G. Kewes, T. Aichele, and O. Benson, Nano Lett., **11**, 198 (2010).
7. C. Liberale, P. Minzioni, F. Bragheri, F. De Angelis, E. Di Fabrizio, and I. Cristiani, Nat. Photon., **1**, 723 (2007).
8. M. Pisco, F. Galeotti, G. Quero, A. Iadicicco, M. Giordano, and A. Cusano, ACS Photon., **1**, 917 (2014).
9. C. H. Lin, S. C. Lei, W. H. Hsieh, Y. C. Tsai, C. N. Liu, and W. H. Cheng, Opt. Express, **25**, 24480 (2017).
10. R. Marchetti, C. Lacava, L. Carroll, K. Gradkowski, and P. Minzioni, Photon. Res., **7**, 201 (2019).
11. H. Kihm and S. W. Kim, Opt. Lett., **29**, 2366 (2004).
12. H. Bae, X. M. Zhang, H. Liu, and M. Yu, Opt. Lett. **35**, 1701 (2010).
13. B. Liu, J. Lin, J. Wang, C. Ye, and P. Jin, IEEE Photon. Tech. Lett., **28**, 581 (2016).
14. W.C. Young, V. Shah, and L. Curtis, IEEE Photon. Tech. Lett., **1**, 461 (1989).
15. Y. J. Kim, U. C. Paek, and B. H. Lee, Opt. Lett., **27**, 1297 (2002).

References

1. R. X. Yan, J. H. Park, Y. Choi, C. J. Heo, S. M. Yang, L. P. Lee, and P. D. Yang, "Nanowire-based single-cell endoscopy," Nat. Nanotechnol., 7, 191-196 (2012).
2. R. X. Yan, D. Gargas, and P. D. Yang, "Nanowire photonics," Nat. Photon., 3, 569-576 (2009).
3. J. H. Chen, Q. Jing, F. Xu, Z. D. Lu, and Y. Q. Lu, "High-sensitivity optical-fiber-compatible photodetector with an integrated CsPbBr3-graphene hybrid structure," Optica, 4(8), 835-838 (2017).
4. P. C. Debnath, S. Uddin, and Y. W. Song, "Ultrafast all-optical switching incorporating in situ graphene grown along an optical fiber by the evanescent field of a laser," ACS Photon., 5(2), 445-455 (2018).
5. F. M. Xie, N. Yao, W. Fang, H. F. Wang, F. X. Gu, and S. L. Zhuang, "Single-mode lasing via loss engineering in fiber-taper-coupled polymer bottle microresonators," Photon. Res., 5(6), B29-B33 (2017).
6. T. Schröder, A. W. Schell, G. Kewes, T. Aichele, and O. Benson, "Fiber-integrated diamond-based single photon source," Nano Lett., 11(1), 198-202 (2010).
7. C. Liberale, P. Minzioni, F. Bragheri, F. De Angelis, E. Di Fabrizio, and I. Cristiani, "Miniaturized all-fibre probe for three-dimensional optical trapping and manipulation," Nat. Photon., 1(12), 723-727 (2007).
8. M. Pisco, F. Galeotti, G. Quero, A. Iadicicco, M. Giordano, and A. Cusano, "Miniaturized sensing probes based on metallic dielectric crystals self-assembled on optical fiber tips," ACS Photon., 1(10), 917-927 (2014).
9. C. H. Lin, S. C. Lei, W. H. Hsieh, Y. C. Tsai, C. N. Liu, and W. H. Cheng, "Micro-hyperboloid lensed fibers for efficient coupling from laser chips," Opt. Express, 25(20), 24480-24485 (2017).
10. R. Marchetti, C. Lacava, L. Carroll, K. Gradkowski, and P. Minzioni, "Coupling strategies for silicon photonics integrated chips," Photon. Res., 7(2), 201-239 (2019).
11. H. Kihm and S. W. Kim, "Nonparaxial free-space diffraction from oblique end faces of single-mode optical fibers," Opt. Lett., 29(20), 2366-2368 (2004).
12. H. Bae, X. M. Zhang, H. Liu, and M. Yu, "Miniature surface-mountable Fabry-Perot pressure sensor constructed with a 45° angled fiber," Opt. Lett., 35(10), 1701-1703 (2010).
13. B. Liu, J. Lin, J. Wang, C. Ye, and P. Jin, "MEMS-based high-sensitivity Fabry-Perot acoustic sensor with a 45° angled fiber," IEEE Photon. Tech. Lett., 28(5), 581-584 (2016).
14. W.C. Young, V. Shah, and L. Curtis, "Loss and reflectance of standard cylindrical-ferrule single-mode connectors modified by polishing a 10° oblique end-face angle," IEEE Photon. Tech. Lett., 1(12), 461-463 (1989).
15. Y. J. Kim, U. C. Paek, and B. H. Lee, "Measurement of refractive-index variation with temperature by use of long-period fiber gratings," Opt. Lett., 27(15), 1297-1299 (2002).